Enhanced Photocatalytic Activity and Antiviral Evaluation of CuO@Fe_2O_3 NC for Amoxicillin Degradation and SARS-CoV-2 Treatment

Laouini Salah Eddine [1,2],Souheila Legmairi[1,], Souhaila Meneceur[2],Gamil Gamal Hasan[2*], , Hamdi Ali Mohammed[1]

[1] Laboratory of Biotechnology Biomaterial and Condensed Matter, Faculty of Technology, University of El Oued, 39000 El-Oued, Algeria
[2] Department of Process Engineering, Faculty of Technology, University of El Oued, 39000 El-Oued, Algeria

Abstract

Copper oxide nanoparticles (CuO NPs) and CuO NPs decorated with hematite (Fe_2O_3) nanocomposites (CuO@Fe_2O_3 NC) were biosynthesized by a green method using *Portulaca oleracea* leaves extract. The NC were characterized using various techniques, including X-ray diffraction (XRD), Fourier transform infrared (FTIR) spectroscopy, scanning electron microscopy (SEM), energy-dispersive X-ray spectroscopy (EDS), and UV-Vis spectroscopy. The results showed that the synthesized CuO and CuO@Fe_2O_3 NC were crystalline with a monoclinic crystal structure and contained functional groups responsible for catalytic activity. The size of the nanocomposites ranged from 39.5 to 45.9 nm, and they exhibited a variety of agglomerated or aggregated shapes. The CuO@Fe_2O_3 NC showed improved photocatalytic activity for the degradation of antibiotics in water and wastewater and promising antiviral activity against SARS-CoV-2, indicating its potential for use in disinfection applications. The study investigated the impact of irradiation time on the photocatalytic degradation of Amoxicillin and found that increasing the irradiation time led to a higher degradation rate. The band gap energy (Eg) for pure CuO NPs was around 2.4 eV and dropped to 1.6 eV with CuO@Fe_2O_3 NC. In summary, the CuO@Fe_2O_3 NC has the potential to be an efficient photocatalyst and promising antiviral agent for environmental remediation. The CuO@Fe2O3 nanocomposites have been found to possess a high degree of efficacy in inactivating SARS-CoV-2 infectivity. The results of the study indicate that the nanocomposites exhibit potent anti-viral properties and hold significant potential for use in mitigating the spread of the virus.

Keywords: Nanocomposite, CuO nanoparticles, Fe2O3 nanoparticles, antibiotic degradation, antiviral activity

1. Introduction

Nanotechnology has emerged as a prominent area of research in recent times. Starting from the 1970s with the inception of nanoscience, this scientific field has garnered significant interest among scholars and has expanded considerably in terms of research activities (1).

Nanotechnology involves a multidisciplinary approach to studying particles whose size is measured in parts per billion (10^{-9}), typically ranging from 1 to 100 nanometers (2, 3). Various types of nanostructures, including nanoparticles (NPs), nanotubes, and nanopores, exhibit intriguing properties that can be utilized in diverse industrial applications depending on their synthesis method and intended purpose (4). Metal nanoparticles (NPs) have been recognized for their significant properties, particularly as catalysts, biosensors, drug delivery vehicles, bio-imaging agents, supplements in the pharmaceutical and food industries, and in the textile industry (5).

CuO, a promising p-type semiconductor, has attracted significant interest for its remarkable optical, electrical, physical, and magnetic characteristics. Its versatile applications, including catalysis, make it widely utilized (6), solar energy conversion (7), gas sensor (8), and field emission. CuO is a semiconductor substance with a narrow band gap of 1.4 eV, is a non-toxic substance that is widely available (9). It has been extensively researched for its photoconductive and photochemical properties, particularly in relation to its potential applications in photocatalysis under visible light irradiation. Furthermore, due to its unique characteristics of a high affinity for organic dyes or antibiotics and a large surface to volume ratio, CuO is also employed as an effective absorbent for removing organic dyes or antibiotics over a wide pH range (10). However, There is a wide range of methods used to synthesize metal nanoparticles (NPs), from physical to chemical means, which can be resource-intensive and require expensive equipment. Additionally, these methods may involve the use of hazardous chemicals, leading to environmental issues and toxicities. Consequently, scientists have been concentrating on discovering a more optimal solution for NP synthesis, which has resulted in the adoption of a biological approach using green technologies.(11-13). This method employs biological agents, including medicinal plants, microorganisms, and isolated natural compounds, as reducing and stabilizing agents to achieve its objectives (2). The implementation of this environmentally friendly technique has resulted in the discontinuation of extensive usage of hazardous organic

compounds(14), improved productivity, lowered toxicity and ecological hazards, and reduced costs compared to prior physical and chemical methodologies (15).

Purslane (*Portulaca oleracea* L.) is an herbaceous, succulent, and annual weed that is widely distributed in both tropical and temperate regions around the world. This plant has been used for both medicinal and culinary purposes in China for thousands of years. Purslane is rich in nutrients such as proteins and carbohydrates. It holds great importance as a traditional Chinese medicine due to its exceptional medicinal properties, particularly in the treatment of dysentery with bloody stools, and for external application in cases of boils, sores, eczema, erysipelas, insect and snake bites (16). Every component of the plant contains compounds that act as effective reducing agents for metal ions. The impact of extracts from different parts of the plant, including the stem, leaves, and roots, on the size of nanoparticles (17, 18). The emergence of new strains of viruses and their resulting outbreaks pose a significant threat to humanity (19). The COVID-19 pandemic, caused by SARS-CoV-2, has had a profound impact on global health and economy, bringing many aspects of life to a standstill (19). Continuous evolution of new viruses poses a global challenge, necessitating the development of innovative methodologies, besides the search for new antiviral drugs, to enhance the efficacy of existing drugs and other viral control approaches(20). Vaccinations represent an economical strategy that has substantially decreased the prevalence of viral diseases. (21). Therefore, emerging strategies are being widely employed to improve the efficacy of vaccines (22). Nanotechnology-based approaches have recently emerged as promising antimicrobial and antiviral agents (23, 24). These approaches include antiviral facemasks, textiles, and coatings that can potentially eliminate viruses upon contact with surfaces. Several studies have demonstrated the potential of nanoparticles in augmenting cellular immunity by enhancing the action of antigens (25). CuO and Fe_2O_3 nanoparticles, synthesized through a green method that utilizes plant extracts, exhibit antiviral properties against the Newcastle Disease Virus (NDV) and SARS-CoV-2, Their noteworthy biophysicochemical features allow for the protection of antigens from degradation and targeted delivery to relevant antigens-introducing cells and sub-cellular components (26-28). Furthermore, the plant extract-based approach to nanoparticle synthesis incorporates various natural substances, leading to higher purity of the resulting nanoparticles(29).

In the present study, we investigated the potential of a nanocomposite consisting of copper oxide and iron oxide hematite ($CuO@Fe_2O_3$ NC) as an adsorbent for removing antibiotics from water and wastewater. We used various analytical techniques including FTIR, XRD, SEM, and UV-Vis spectrometry to characterize the CuO and $CuO@Fe_2O_3$ NC. The impact of irradiation time on the degradation of amoxicillin was also evaluated. Additionally, we evaluated the antiviral activity of the nanocomposite against SARS-CoV-2. Our study is the first to report on the use of $CuO@Fe_2O_3$ NC as an adsorbent for removing antibiotics and as an antiviral agent against SARS-CoV-2.

2. Material and methods

Copper sulphateII pentahyrated ($CuSO_4{\cdot}5H_2O$, 98%, Sigma-Aldrich) was used as precursor, sodium hydroxide (NaOH), $Fe(NO_3)_3.9H_2O$(98%, Sigma-Aldrich) The chemicals were utilized as obtained without additional refinement. Before being utilized, all glassware underwent cleaning with doubly distilled water and drying in a hot air oven. To generate copper oxide nanoparticles (CuO NPs), plant leaves obtained from district El-oued (located in the southeast region of Algeria at coordinates 330 07"00" N 70 11"00" E) were collected and utilized as a source of reducing and stabilizing agents. This selection is based on studies carried out on this plant in the VTRS laboratory. MB dye was supplied by LOBA CHEMIE, India.

2.1.Preparation of purslane Portulaca oleracea Leaf Extract

To prepare a Portulaca oleracea leaf extract solution, the leaves were first cleaned, dried, and finely diced, weighing 100 g in total. The diced leaves were boiled in 100 mL of de-ionized water in a 250 mL Erlenmeyer flask for five minutes at a temperature of 80°C, followed by cooling to room temperature. The resulting solution was then filtered through a filter paper to remove any solid particles and subsequently passed through a Whatman filter paper, which had a pore size of 0.2 µm. The filtrate obtained was kept as a stock solution for synthesizing CuO NPs and stored at 4°C until further use.

2.2.Green Synthesis of CuO NPs

To synthesis CuO nanoparticles, a 1000 mL Erlenmeyer flask was used to combine 500 mL of 1 mM $CuSO_4{\cdot}5H_2O$ solution with 500 mL of *Purslane leaf* extract. The mixture was stirred continuously at 70°C for 5 hours and the color of the solution changed from deep blue to colorless, then to brick red and dark red. Afterward, The solution containing CuO nanoparticles was subjected to centrifugation at room temperature using a Beckman centrifuge with a Beckman JA-17 rotor, at a speed of 5000 rpm for 10 minutes. The resultant mixture was collected, and the supernatant was discarded. The collected CuO nanoparticles were then dried on a watch glass and subjected to annealing at 400°C for a duration of 3 hours, to obtain the final product. The resulting black precipitate was ground for further analysis.

2.3.Synthesis of $CuO@Fe_2O_3$ NC Nanocomposites

During the experiment, 0.8 grams of copper oxide nanoparticles were dispersed in 70 milliliters of distilled water and carefully stirred for two hours. Next, 70 milliliters of a 0.01 M solution of iron nitrate was added to the mixture, and it was

continuously stirred for an additional two hours while adding 5 mL of 0.1 M NaOH until the color of the solution changed from black to brown. The resulting brown precipitate was then centrifuged for 10 minutes at 3000 rpm and washed multiple times with deionized water. The resulting brown powder was dried in an oven at 100 °C and finally annealed at 400 °C for three hours to produce copper oxide nanoparticles decorated with iron oxide hematite, which are referred to as CuO@Fe_2O_3 NC.

2.4.Characterization

Various techniques were employed to investigate the optical, chemical, and morphological features of CuO and CuO@Fe_2O_3 NC nanoparticles that were synthesized. The crystalline structure of the biosynthesized nanoparticles was studied through X-ray diffractometry (XRD) in the 2-theta (2θ) range of 20-80 using a Rigaku Miniflex 600 device with Cu-Kα (λ=1.5406 Å) radiation. The shape of CuO and CuO@Fe_2O_3 NC particles was determined using a scanning electron microscope (SEM-TESCAN VEGA microscope) operating at a voltage of 10 kV. Fourier transforms infrared (FTIR) spectroscopy, which employed a Thermo Fisher Scientific Nicolet iS5 device in the range of 400 to 4000 cm^{-1}, was used to identify the different functional groups present in the plant leaves extract and the biosynthesized nanoparticles. Additionally, the optical properties of CuO and CuO@Fe_2O_3 NC were studied using UV-Vis spectroscopy (Shimadzu UV-Vis device) in the range of 200 to 900 nm.

2.5.Photocatalytic activity

The photocatalytic performance of the photocatalyst was assessed using an aqueous solution of Amoxicillin (AMOX). To evaluate the degradation of the AMOX solution under sunlight exposure, a UV-Vis spectrophotometer was utilized. A specific quantity of the nanocomposite was prepared and mixed with a 2.5□10-5 M AMOX solution. The mixture was then allowed to equilibrate through agitation in the dark for a minimum of 30 min to achieve adsorption-desorption equilibrium. Subsequently, the solution was continuously stirred and exposed to sunlight. At predetermined intervals, analytical samples were collected and subjected to centrifugation and filtration to eliminate the photocatalyst. The AMOX in each sample was then measured over time using a UV-Vis spectrophotometer at λmax=228 nm. The percentage of degradation was calculated using the provided formula(30):

$$\text{Degradation (\%)} = ((A0-At)/A0)\times 100 \qquad (1)$$

Where The variables A0 and At denote the initial absorbance of the AMOX solution (at time zero) and the absorbance of the AMOX solution after a designated duration of time (at time t), respectively.

2.6. Fluorescent qPCR

The collected oropharyngeal swab samples were subjected to a control test using Fluorescence quantitative PCR. To prepare the sample, an eluent was first centrifuged at a speed of 12,000 rpm for 5 min, and the resulting precipitate was mixed with 1 ml of sterilized saline before being centrifuged again at 12,000 rpm for five minutes. The supernatant was discarded, and the remaining precipitate was mixed with a 50 l lysate solution containing 1 M Tris-HCL pH 8.0, 1 mmol/L EDTA, and 1% TritonX-100. The mixture was then heated to a constant temperature of 100 °C for 10 minutes, and subsequently centrifuged at 10,000 rpm for 5 minutes. The resulting supernatant was used for testing with the M. pneumoniae nucleic acid detection kit (DaAn Gene Co., Ltd. Guangzhou) and ABI7500 fluorescence quantitative PCR instrument (Thermo Fisher Scientific, USA), following the kit instructions with strict adherence to operational protocols.

2.7.EasyNAT Assay

After fully mixing the oropharyngeal swab sample with the MP-DNA extraction solution, the remaining portion was combined with the MP cartridge. The nucleic acid analyzer's scanning area, which was aimed at the two-dimensional code on the detection tube, was utilized to evaluate information from the tube. To initiate the test, the detection tube was placed in the sample chamber of the nucleic acid analyzer, and the test was started by closing the sample chamber lid and clicking the start button. Following the completion of the test cycles, the instrument automatically displayed and recorded the test results.

2.8. SARS-CoV-2 Detection by RT-qPCR

تعليق عليه [JA1]: Use this picture insteed.

Individuals for the cases and controls were selected based on the results of RT-qPCR assays conducted at the Regional Laboratory of Medical Analysis El Madjed in Eloued, Algeria. The PCR analyses were carried out using the SARS-CoV-2 PCR Kit, manufactured by Lifotronic, China, which consisted of primers and probes specifically designed for detecting SARS-CoV-2, as well as an internal control (RNAsa P) that emitted fluorescent signals in the green (FAM: 470-510 nm) and orange (VIC: 585-610 nm) channels. Samples with cycle threshold (Ct) values < 37 (FAM) and Ct < 40 (VIC) were considered positive, in accordance with the manufacturer's instructions.

3.Result and discussion

3.1.UV-vis spactrophmetre

The UV-Vis absorption spectra of pure CuO and CuO@Fe_2O_3 NC are presented in **Figure 1**, which depicts the variation of absorption as a function of wavelength in the 200-800 nm range. In **Figure 1.a**., it can be observed that both CuO and CuO@Fe_2O_3 NC exhibit significant absorption at 366 nm while displaying low absorption in the visible spectrum. This can be attributed to the excitation of lower energy state molecules to higher energy levels, resulting in the absorption of more photon energy. The determination of the optical band gap (Eg) is performed using a Tauc plot (2) based on the following relationship:

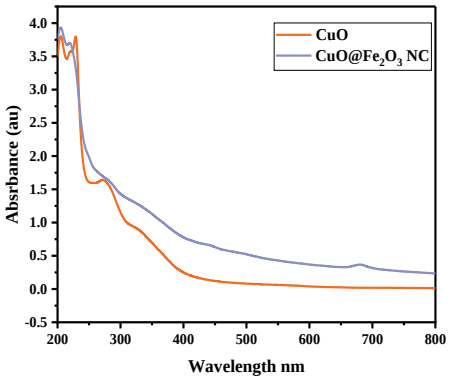

Figure 1. (a). Uv-vis spectra of CuO and CuO@Fe_2O_3 NC (b). Their corresponding gap energy.

$$\propto=(A(hv-Eg)^{1/2})/hv \quad (2)$$

In the case of permitted direct transition(31) , the value of "n" is ½, while "h" refers to constant Plank, "v" is the frequency of light radiation, and "Eg" is the energy band gap. $(hv)^{1/2}$ vs (hv) curves are constructed for CuO and CuO@Fe_2O_3 NC. By extrapolating the

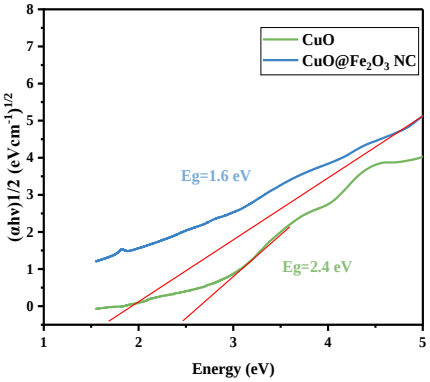

linear portions of these curves along the x-axis, the energy band gap (Eg) can be obtained. The results presented in **Figure 1.b** indicate that the band gap energy (Eg) for pure CuO NPs is approximately 2.4 eV, while it decreases to 1.6 eV for CuO@Fe2O3 NC. This decrease is attributed to strong quantum confinement and an increase in the surface/volume ratio, which causes the band gap to narrow. The reduction in the band gap energy (Eg) confirms the presence of Fe3+ on the Cu2+ surface of the CuO lattice. The interaction between CuO and Fe2O3 in the nanocomposite may contribute to the shift in the absorption spectrum and the corresponding decrease in bandgap.

تعليق عليه [JA2]: Revise these values according to the new Figure that will be included

3.2.XRD analysis

The XRD patterns of CuO and CuO@Fe_2O_3 NC are shown in **Figure 2.** demonstrates that the CuO nanoparticles are in a crystalline form and are identical to pure CuO, indicating the formation of a single-phase CuO with a monoclinic structure (32). In the present work, the diffraction patterns were observed to be at 2θ = 32, 35, 38.9, 48.7, 53, 58, 61, 66, 68 and 75 ° were assigned to the reflection lines of monoclinic CuO nanoparticles related to (-110), (002), (200), (-202), (020), (202), (-113), (-311), (-220) and (-220), respectively crystal planes of CuO with lattice parameters of a =4.6853 Å, b = 3.4257 Å, c = 5.1303 Å and C2/c spacing group according (JCPDS card No: 00-045-0937). The XRD pattern illustrates well-defined narrow peaks showing that the biosynthesized CuO nanoparticles are highly pure. The results were found to deal with the reported diffraction patterns of CuO NPs prepared by Das et al. (33). The XRD pattern of CuO@Fe_2O_3 NC show a only one peak at 31º. This peak could be attributed to the (202) crystallographic plane of hematite (Fe_2O_3), which corresponds to about 95% of the trigonal structure. Based on the results, it was observed that the average crystal size for CuO NPs was 26.46 nm,

تعليق عليه [JA3]: https://doi.org/10.3390/ma16051798

تعليق عليه [JA4]: The new values (recalculated values) should be included.
According to the CuO@Fe2O3 pattern, the averages is 26. 79 nm. Therefore, the average crystalline size of CuO alone shoul be smaller.

تعليق عليه [JA5]: This is a perfect response to the reviewer's comment. However, it is important to explain the symbols included in the Figure within the same box, clearly indicating the CuO and Fe2O3 phases. Additionally, it should be mentioned that the reported size is calculated as the average of all the peaks. This clarification will provide a more comprehensive understanding and convey the reviewer.

تعليق عليه [JA6]: I have calculated the average size of the CuO@Fe2O3 and it is found to be 26.79 nm.
Therefore, including the crystalline size for each peak in the CuO pattern will facilitate the comparison.

whereas for CuO/Fe2O3 composite, it was 30.14 nm. To facilitate better comparison, Figure 2 also includes the crystalline size and oxide phase information at each peak.

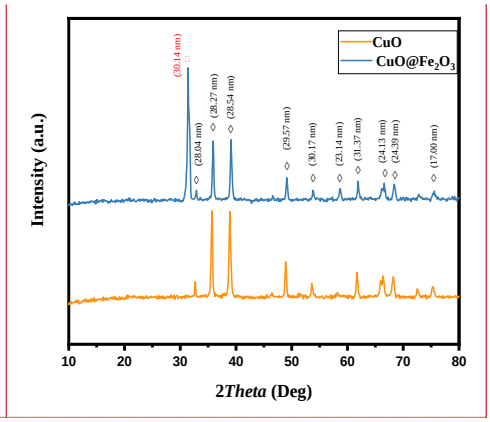

Figure 2. XRD patterns for the biosynthesized CuO and CuO@Fe_2O_3 NC.

3.3. Morphological Analysis

تعليق عليه [JA7]: Replace the Figure 3d according to Reviewer comment

The surface morphologies of the samples were investigated using field effect scanning electron microscopy (SEM).

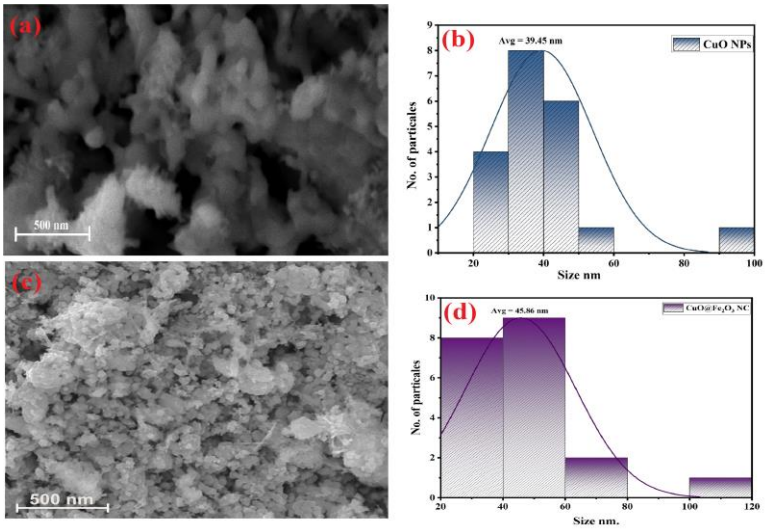

Figure 3. SEM analysis of the biosynthesized nanoparticles: (a). CuO NPs and (c) CuO@Fe_2O_3 NC nanocomposite (b and d) their corresponding crystallite size distributions.

SEM images in **Figure 3.a** reveal that CuO NPs exhibit a variety of agglomerated or aggregated shapes, including spherical, cubic, and elongated structures.

After decoration with Fe_2O_3, the resulting CuO@Fe_2O_3 NC composite particles were found to be even more agglomerated or aggregated, potentially due to the interaction of the magnetic properties of Fe_2O_3 and the electron beam from the SEM source, as well as the competition of reducing agents (such as polyphenols) on the surface of both CuO and Fe_2O_3 **(Figure 3.c)**. The particle size distribution histograms for the CuO NPs and CuO@Fe_2O_3 NC are shown in **Figure 3.b** and d, respectively. The data analysis conducted using SEM revealed that the average distribution of particle sizes for the CuO and CuO@Fe2O3 NC was approximately 39.5 nm and 45.9 nm, respectively.

The nanocomposite contains iron, oxygen, and copper elements, which are confirmed by the energy-dispersive spectra (EDS) analysis of the samples scattered across the copper grids coated with amorphous carbon (**Figure 4. a** and **b**). The EDS analysis reveals that the atomic percentages of O and Cu are 58 and 41, respectively, respectively. Moreover, the atomic percentages of Fe, Cu, and O are 10, 4, and 7, respectively. These results are in excellent agreement with the findings of the X-ray diffraction (XRD) study, which confirms the sample's purity and the absence of any unexpected elements. Additionally, the observed size distribution in the scanning electron microscopy (SEM) images aligns with the anticipated behavior of the combined CuO@Fe2O3 nanocomposite, demonstrating an increase in size.

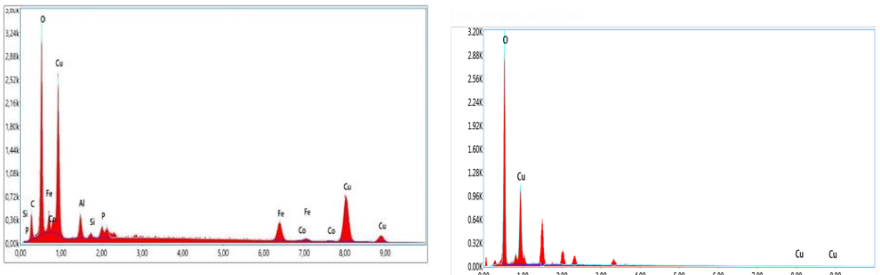

Figure 4. The energy-dispersive spectra of biosynthesized CuO NPs (b). CuO@Fe_2O_3 NC of (a).

3.4. Fourier Transform Infrared (FTIR) Spectroscopy

The identification of flavanones and terpenoids in the extract of Portulaca oleracea leaves was accomplished through the use of FTIR analysis. These compounds are responsible for stabilizing copper oxide nanoparticles, which were biosynthesized and vacuum-dried. The absorption spectra of these nanoparticles can be found in **Figure 5**, with the bonds related to stretching vibrations in primary and secondary amines located at approximately 3408 and 2968 cm−1, respectively (34). The C-H stretching aldehydes were identified by a broad and strong absorption band located at 2162 cm^{-1} (35). The spectroscopic peaks observed at 1440, 1634, and 1734 cm−1 signify the presence of C–C groups originating from aromatic rings, phenols, and the stretching vibration of conjugated carbonyl (–C=O) groups, respectively. These molecular groups may have originated from the pteridophyte cell present in the plant extract (6). The movement of the maximum point in the vicinity of 1600 cm^{-1} on the spectrum was ascribed to the attachment of a C=O moiety to the nanoparticles (36). Concurrently, the peaks detected in the range of 1038-1234 cm^{-1} via FTIR were indicative of the amide III band pertaining to the random coil configuration of the protein (37). During the synthesis of CuO nanoparticles, a band at 873 cm−1 was previously observed, which corresponds to the bending vibrational movements in amides II (38). In the range of 700-400 cm^{-1}, three IR absorption peaks were observed, which indicated the vibrational modes of CuO nanostructures (39). The peak observed at 598 cm^{-1} is likely attributed to the stretching of Cu-O, and it corresponds to the (B2u mode) (39, 40).Absorption peaks in 900–700 cm^{-1} were also attributed to the bending vibration (aromatic) of C–H group (41). Nevertheless, some interesting observations were made during the FTIR analysis. For instance, the disappearance of the IR peak around 1200 cm-1 in the CuO/Fe2O3 composite, compared to CuO, can be attributed to the formation of the

CuO/Fe2O3 nanocomposite. The interaction between CuO and Fe2O3 can cause changes in the vibrational modes and bonding characteristics of the materials, leading to shifts or disappearances of specific IR peaks..

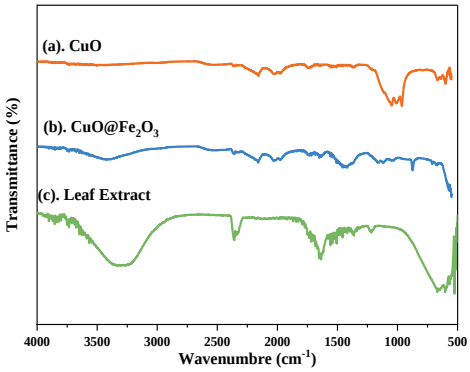

Figure. 5. FT-IR spectrum of Biosynthesized (a) CuO NPs (b) $CuO@Fe_2O_3$ NC and (c) Portulaca oleracea leaf extract.

3.5. Thermogravimetric Analysis (DSC–TGA)

Thermogravimetric analysis is a method that entails subjecting a substance to high temperatures, causing the bonds connecting the molecules to weaken and eventually break. As the reaction initiates, the weight of the sample gradually decreases, followed by a rapid decline over a relatively narrow temperature range. The process levels out when the reactants become depleted. The shape of the TGA curve is mainly determined by the kinetics parameters [39]. The DSC and TGA methods are utilized to observe the alterations in the properties of the sample caused by fluctuations in temperature. These changes are primarily of a physicochemical nature. The biosynthesized $CuO@Fe_2O_3$ NC nanocomposite-based product was subjected to a heating rate of 10°C/min, and its typical DSC/TGA curves were recorded in **Figure 6**. The thermogram illustrates the thermal behavior and stability of CuO@Fe2O3 NC. The sample mass loss resulting from polysaccharide breakdown was measured to be approximately 1.6% of the total mass at an onset temperature of around 539.7 °C, during heating from 100 to 1100 °C at a rate of 10 °C/min. Consequently, it appears that annealing at temperatures higher than 539.7°C can ensure the production of a stable CuO@Fe2O3 NC.

The DSC plot of the product based on the biosynthesized CuO@Fe2O3 NC exhibits a solitary endothermic peak, which is centered at around 539 °C (Figure 6). The sample undergoes a phase transition in the range of 100°C to 600°C. It is evident that a prominent peak occurs at 684.27 °C, which may represent the melting point of the CuO@Fe2O3 NC. The observed peak at this temperature could be attributed to the conversion of copper oxide and iron complex into a nanocomposite consisting of copper hydroxide and iron hydroxide. This suggests that the reaction at this temperature may involve the transformation of CuO and Fe2O3 into different crystalline phases, potentially including the formation of copper hydroxide and iron hydroxide. To validate this hypothesis, further investigation in the future is needed, which could involve conducting XRD analysis of the products below and above this temperature to obtain more comprehensive data.

تعليق عليه **[JA8]:** Reference with different style.

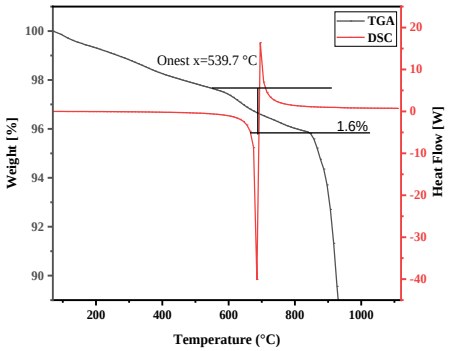

Figure 6. DSC-TGA plot of CuO@Fe_2O_3 NC

3.6. Photocatalytic activity

The present study investigated the photodegradation of Amoxicillin pharmaceutical using CuO NPs and CuO@Fe_2O_3 NC under sunlight irradiation. The degradation rate of amoxicillin was evaluated by monitoring the change in time (10, 20, 30, 40, 50, and 60) at λmax = 228 nm. The results depicted in **Figure 7b, c** demonstrated that CuO@Fe_2O_3 NC had a higher adsorption percentage within the first 10 minutes of the process compared to CuO NPs, with a percentage of 46.9%, and reached a maximum degradation rate of 98.9% at 60 min (**Figure 7a, c**). In contrast, CuO NPs showed a gradual increase in degradation rate with a value of 29.5% at 10 min and 98.1% at 60 minutes. It was observed that the removal rate of amoxicillin by CuO NPs was significantly slower than CuO@Fe_2O_3 NC, which could be attributed to the larger surface area of CuO@Fe2O3 NC, making it more efficient in photocatalysis. The study measured the reaction rate of CuO NPs and CuO@Fe2O3 NC with AMOX. The rate constant was determined to be k = 0.0608 min−1 for CuO NPs, which was lower than the rate constant for CuO@Fe2O3 NC (k = 0.0696 min−1), indicating that CuO@Fe2O3 NC exhibited better catalytic efficiency (**Figure. 7d**). This improved efficiency was attributed to the synergistic effects of CuO and Fe_2O_3 NPs and the high surface area of CuO@Fe_2O_3 NC. These findings suggest that CuO@Fe_2O_3 NC can be an excellent catalyst for similar reactions.

Equations (3–9) display the mechanism for enhanced photocatalytic activity CuO@Fe_2O_3 NC under sunlight radiations. Under solar irradiation, the transfer of electrons from the valence band (VB) to the conduction band (CB) of CuO@Fe_2O_3 NC results in an energy level higher than the band gap of CuO@Fe_2O_3 NC (1.6 eV), leading to the creation of valence band holes (h^+) and conduction band electrons (e^-)(42). Photogenerated holes in the valence band may directly oxidize antibiotics (OH^-) while oxygen molecules (O_2) adsorbed on the surface of CuO@Fe_2O_3 NC may be transformed into superoxide radicals by the photoelectrons in the conduction band (O^-e). As a result, both the antibiotics metronidazole and cephalexin may be destroyed by photocatalytic O^-_2 and OH [40-42].

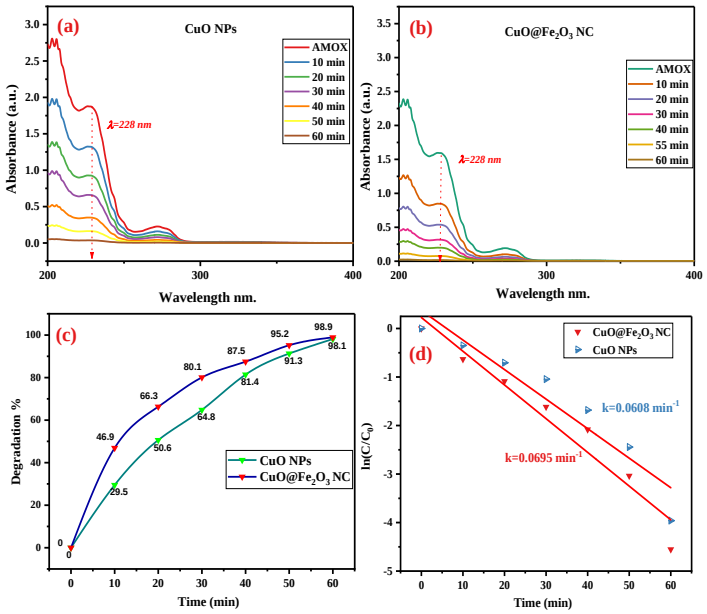

.

Figure 7. Influence of contact time on the degradation efficiency of antibiotics using CuO NPs CuO@Fe2O3 Nanocomposite: (a) Effect of CuO NPs, (b) Effect of CuO@Fe2O3 NC, and (c) degradation rate (d) First-order kinetic plot of ln(c/c0).

Figure 8. Depicts the underlying principle of the Langmuir isotherm model, which suggests that when AMOX is adsorbed onto the surface of CuO@Fe_2O_3 NC, it forms a single layer without any additional stacking of the adsorbate. According to the Langmuir model, a state of equilibrium is attained between the adsorbed AMOX molecules on the NC and the unbound AMOX ions present in the liquid phase.

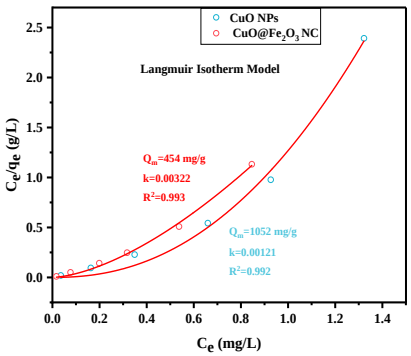

Figure 8. Langmuir isotherm model of Amoxicillin (AMOX) on CuO NPs and CuO@Fe_2O_3 NC

3.7. Antiviral Activity

The EasyNAT System measures the fluorescent signals generated during the run and analyzes the change in fluorescent signals over time to determine the EasyNAT test results. The EasyNAT System uses the measurement of the change in fluorescent signals over time (Tt) to determine if a sample is positive or negative for the presence of SARS-COV-2. The EasyNAT System performs the following steps automatically during sample processing:

The Tt value is amplification time (in minutes) of when the fluorescence value meets the threshold value. The EasyNAT System displays the result for the sample and also includes the Tt values for the ORF 1ab (CoV101), N gene (CoV10r) and GDAPH Internal Control (ICI and ICr) and reports positive or negative results by the following criteria:

- If the Tt value of gene ORF1ab is N/A, test result for gene ORF1ab will be 'Negative'. If the Tt value of gene ORFlab is ≤27, test result for gene ORFlab will be 'Positive'.
- If the Tt value of gene N is N/A, test result for gene N will be 'Negative'. If the Tt value of gene N is ≤27, test result for gene N will be 'Positive'.
- If the Tt value of the IC is N/A, test result for the corresponding IC will be 'Negative'. If the Tt value of an IC is ≤27, test result for the corresponding IC will be 'Positive'.

The **Table 1** shows the Tt values when for the two samples tested using the CuO NPs and CuO@Fe_2O_3 NC. However, at case (after covid) it is clearly appear the existence the influence of both CuO NPs and CuO@Fe_2O_3 NC, the idecate the ability of the biosynthesis to prevent intrcation between the human cell and the virus.

Table 1 Effect of CuO and CuO@Fe_2O_3 NC on SARS CoV-2

		CuO NPs	CuO@Fe_2O_3 NC
Before Covid (positive)	CoV10l	14.22	14.50
	CoV10r	12.32	14.00
	ICI	07.32	NA
	ICr	06.22	NA
After Covid (negative) V/3V 15 min	Cov10l	NA	NA
	Cov10r	NA	NA
	ICI	NA	NA
	ICr	13.00	14.5

- OR1ab(CoV10l)
- N gene (CoV10r)
- GDAPH Internal Control(ICl and Icr)

3.7.1. Antiviral mechanism

The hypothesis suggests that nanocomposite CuO@Fe_2O_3, which interact with SARS-CoV-2, may impede the virus from attaching to host receptors, resulting in the inhibition of viral infection. Furthermore, these interactions may cause irreversible alterations to the virus structure, leading to a decrease in infection. Nanomedicine is a medical application of nanoscale materials, and it includes the development of treatments for viral infections like COVID-19. Nanomedicine has the potential to combat the coronavirus in various ways, such as targeting viral entry. The coronavirus gains entry into human cells through binding with the ACE2 receptor on the cell surface. Nanoparticles can be created to mimic the ACE2 receptor, which would bind to the virus, preventing it from infecting human cells (see **Figure 9**).

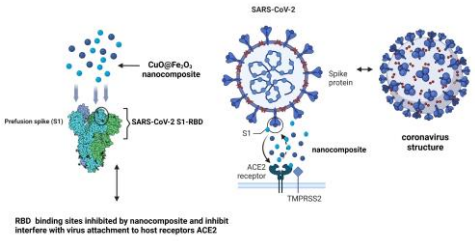

Figure 9. Possible mechanism for SARS-coV-2 using CuO/Fe_2O_3 nanocomposites.

Molecular docking techniques were utilized to validate the interaction between SARS-CoV-2 and a specific nanocomposite. The SARS-CoV-2 protein (6lu7) was sourced from www.pdb.org/pdb/home/home.do, while the nanocomposite was synthesized through the use of Material Studio and Chemdraw software. The protein was prepared using AutoDock Vina and Discovery Studio. Molecular docking is based on the fact that the hybrid nanocomposite CuO@Fe2O3 NC has antiviral activity and has been proven to inhibit SARS-CoV-2 in clinical trials. **Figure 10.** displays the active pocket, which is composed of amino acid residues A:ASP187, A:HIS164, A:CYS145, A:HIS41, A:PRO39, A:ARG40, A:CYS85,

and A:TYR54. The docking results indicate that the interaction between the nanocomposite and target protein was stable, as evidenced by the presence of inter- and intra-hydrogen bonds.

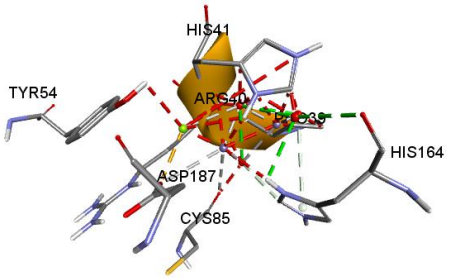

Figure 10. Docking studies of CuO@Fe_2O_3 NC with the binding mode of composite inside the receptor active sites (PDB 6LU7) and the receptor active sites.

4. Conclusion

The fusion of CuO photocatalytic properties and Fe2O3 hematite properties resulted in the creation of nanocomposites of CuO and Fe_2O_3. To produce the CuO@Fe_2O_3 NC material, a green approach was taken, whereby fresh *Portulaca oleracea* leaves aqueous extract was utilized. CuO was generated initially, and Fe_2O_3 was subsequently decorated on copper oxides. The green technique was utilized again to calcine the CuO and Fe_2O_3 at 400 °C for three hours to produce the CuO@Fe_2O_3 NC. The XRD, UV-Vis, ATG-DSC, SEM, and FT-IR spectroscopies were utilized to gain a better understanding of the structural phase of the CuO NPs and CuO@Fe_2O_3 NC nanocomposites. All characterization techniques verified the significant integration of the Fe_2O_3 and CuO compounds, which improved the bandgap and rendered the nanocomposites UV-Visible active when illuminated by visible light. The comprehensive evaluation of CuO@Fe_2O_3 NC nanocomposites' adsorptive and photocatalytic capabilities aimed to completely eradicate the need for antibiotics in wastewater. The results showed that the CuO@Fe_2O_3 NC nanocomposites demonstrated high photocatalytic activity towards amoxicillin antibiotics when compared to only CuO NPs. The improved performance was due to the dispersion of Fe_2O_3 in the CuO structure, which provided uniform active sites for antibiotic adsorption and complete photodegradation. Therefore, the use of CuO@Fe_2O_3 NC catalysts for the removal of various organic pollutants from water is efficient and environmentally beneficial. CuO nanoparticles (NPs) and CuO@Fe_2O_3 nanocomposites have been found to possess the ability to inactivate SARS-CoV-2, the virus responsible for COVID-19. Studies have shown that these materials can effectively reduce the viral load and inhibit the replication of the virus.

References

1. Ijaz I, Bukhari A, Gilani E, Nazir A, Zain H, Saeed R. Green synthesis of silver nanoparticles using different plants parts and biological organisms, characterization and antibacterial activity. Environmental Nanotechnology, Monitoring & Management. 2022;18:100704.
2. Tripathi D, Modi A, Narayan G, Rai SP. Green and cost effective synthesis of silver nanoparticles from endangered medicinal plant Withania coagulans and their potential biomedical properties. Materials Science and Engineering: C. 2019;100:152-64.
3. Ababsa A, Temam HB, Hasan GG, Althamthami M, Malfi N. Effect of sodium dodecyl sulfate and different SiC quantities on electrodeposited Ni-Co alloy coatings. Surface Topography: Metrology and Properties. 2022;10(1):015038.
4. Nadaf SJ, Jadhav NR, Naikwadi HS, Savekar PL, Sapkal ID, Kambli MM, et al. Green synthesis of gold and silver nanoparticles: Updates on research, patents, and future prospects. OpenNano. 2022:100076.
5. Mohammed Mohammed HA, Souhaila M, Eddine LS, Hasan GG, Kir I, Mahboub MS. A novel biosynthesis of MgO/PEG nanocomposite for organic pollutant removal from aqueous solutions under sunlight irradiation. Environmental Science and Pollution Research. 2023:1-10.
6. Altikatoglu M, Attar A, Erci F, Cristache CM, Isildak I. Green synthesis of copper oxide nanoparticles using Ocimum basilicum extract and their antibacterial activity. Fresenius Environ Bull. 2017;25(12):7832-7.

7. Kaneshiro J, Gaillard N, Rocheleau R, Miller E. Advances in copper-chalcopyrite thin films for solar energy conversion. Solar Energy Materials and Solar Cells. 2010;94(1):12-6.
8. Zhang Y, He X, Li J, Zhang H, Gao X. Gas-sensing properties of hollow and hierarchical copper oxide microspheres. Sensors and Actuators B: Chemical. 2007;128(1):293-8.
9. Meshram S, Adhyapak P, Mulik U, Amalnerkar D. Facile synthesis of CuO nanomorphs and their morphology dependent sunlight driven photocatalytic properties. Chemical engineering journal. 2012;204:158-68.
10. Sadeghi Meresht A, Ezzatzadeh E, Dehbandi B, Salimifard M, Rostamian R. Fe3O4/CuO Nanocomposite Promoted Green Synthesis of Functionalized Quinazolines Using Water Extract of Lettuce Leaves as Green Media: Study of Antioxidant Activity. Polycyclic Aromatic Compounds. 2022;42(7):4793-808.
11. Eddine LS, Djamila B, Redha OM. Solvent pH extraction effect on phytochemical composition and antioxidant properties of Algerian Matricaria Pubescens. Journal of Pharmacy Research. 2016;10(2):106-12.
12. Bouafia A, Laouini SE, Tedjani ML, Ali GA, Barhoum A. Green biosynthesis and physicochemical characterization of Fe3O4 nanoparticles using Punica granatum L. fruit peel extract for optoelectronic applications. Textile Research Journal. 2022;92(15-16):2685-96.
13. JAA A, Jiménez-Rosado M, Guerrero A, Romero A. Eco-friendly synthesis of ZnO-nanoparticles using Phoenix dactylifera L. polyphenols: Physicochemical, microstructural and functional assessment. 2022.
14. Hasan GG, Mohammed HA, Althamthami M, Khelef A, Laouini SE, Meneceur S. Synergistic Effect of Novel biosynthesis SnO2@ Fe3O4 Nanocomposite: A Comprehensive Study of Its Photocatalytic, Antibiotic, Antibacterial, and Antimutagenic activities. Journal of Photochemistry and Photobiology A: Chemistry. 2023:114874.
15. Nicolae-Maranciuc A, Chicea D, Chicea LM. Ag nanoparticles for biomedical applications—Synthesis and characterization—A review. International Journal of Molecular Sciences. 2022;23(10):5778.
16. Zhu H, Wang Y, Liu Y, Xia Y, Tang T. Analysis of flavonoids in Portulaca oleracea L. by UV–vis spectrophotometry with comparative study on different extraction technologies. Food Analytical Methods. 2010;3:90-7.
17. Al-Otibi F, Alfuzan SA, Alharbi RI, Al-Askar AA, Al-Otaibi RM, Al Subaie HF, et al. Comparative study of antifungal activity of two preparations of green silver nanoparticles from Portulaca oleracea extract. Saudi Journal of Biological Sciences. 2022;29(4):2772-81.
18. Aboulthana WM, Omar NI, Hasan EA, Ahmed KA, Youssef AM. Assessment of the biological activities of Egyptian purslane (Portulaca oleracea) extract after incorporating metal nanoparticles, in vitro and in vivo study. Asian Pacific Journal of Cancer Prevention: APJCP. 2022;23(1):287.
19. Koven S. They call us and we go. New England Journal of Medicine. 2020;382(21):1978-9.
20. Dickey SW, Cheung GY, Otto M. Different drugs for bad bugs: antivirulence strategies in the age of antibiotic resistance. Nature Reviews Drug Discovery. 2017;16(7):457-71.
21. Haque A, Akçeşme FB, Pant AB. A review of Zika virus: hurdles toward vaccine development and the way forward. Antiviral Therapy. 2018;23(4):285-93.
22. Pardi N, Hogan MJ, Porter FW, Weissman D. mRNA vaccines—a new era in vaccinology. Nature reviews Drug discovery. 2018;17(4):261-79.
23. Milovanovic M, Arsenijevic A, Milovanovic J, Kanjevac T, Arsenijevic N. Nanoparticles in antiviral therapy. Antimicrobial nanoarchitectonics: Elsevier; 2017. p. 383-410.
24. Singh L, Kruger HG, Maguire GE, Govender T, Parboosing R. The role of nanotechnology in the treatment of viral infections. Therapeutic advances in infectious disease. 2017;4(4):105-31.
25. Stewart JM, Keselowsky BG. Combinatorial drug delivery approaches for immunomodulation. Advanced drug delivery reviews. 2017;114:161-74.
26. Yugandhar P, Vasavi T, Jayavardhana Rao Y, Uma Maheswari Devi P, Narasimha G, Savithramma N. Cost effective, green synthesis of copper oxide nanoparticles using fruit extract of Syzygium alternifolium (Wt.) Walp., characterization and evaluation of antiviral activity. Journal of Cluster Science. 2018;29:743-55.
27. Merkl P, Long S, McInerney GM, Sotiriou GA. Antiviral activity of silver, copper oxide and zinc oxide nanoparticle coatings against SARS-CoV-2. Nanomaterials. 2021;11(5):1312.
28. Foka FET, Manamela N, Mufamadi SM, Mufhandu HT. Potential of Azadirachta indica as a Capping Agent for Antiviral Nanoparticles against SARS-CoV-2. BioMed Research International. 2022;2022:5714035.
29. Usman AI, Aziz AA, Noqta OA. Green sonochemical synthesis of gold nanoparticles using palm oil leaves extracts. Materials Today: Proceedings. 2019;7:803-7.
30. Althamthami M, Hachmi GTE, Temam HB, Rahmane S, Hasan GG. Improved Photocatalytic Activity under the Sunlight of High Transparent Hydrophilic Bi-doped TiO2 Thin-films. Journal of Photochemistry and Photobiology A: Chemistry. 2023:114818.

31. Bouafia A, Laouini SE, Khelef A, Tedjani ML, Guemari F. Effect of ferric chloride concentration on the type of magnetite (Fe3O4) nanoparticles biosynthesized by aqueous leaves extract of artemisia and assessment of their antioxidant activities. Journal of Cluster Science. 2021;32(4):1033-41.
32. Vaseem M, Umar A, Kim SH, Hahn Y-B. Low-temperature synthesis of flower-shaped CuO nanostructures by solution process: formation mechanism and structural properties. The Journal of Physical Chemistry C. 2008;112(15):5729-35.
33. Das D, Nath BC, Phukon P, Dolui SK. Synthesis and evaluation of antioxidant and antibacterial behavior of CuO nanoparticles. Colloids and Surfaces B: Biointerfaces. 2013;101:430-3.
34. Cuevas R, Durán N, Diez M, Tortella G, Rubilar O. Extracellular biosynthesis of copper and copper oxide nanoparticles by Stereum hirsutum, a native white-rot fungus from chilean forests. Journal of Nanomaterials. 2015;16(1):57-.
35. Belskaya OB, Danilova IG, Kazakov MO, Mironenko RM, Lavrenov AV, Likholobov VA. FTIR spectroscopy of adsorbed probe molecules for analyzing the surface properties of supported Pt (Pd) catalysts. Infrared Spectroscopy in Materials Science, Engineering and Technology, PT Theophile, Ed, ed: InTech. 2012.
36. Kannan R, Stirk W, Van Staden J. Synthesis of silver nanoparticles using the seaweed Codium capitatum PC Silva (Chlorophyceae). South African Journal of Botany. 2013;86:1-4.
37. Cai S, Singh BR. A distinct utility of the amide III infrared band for secondary structure estimation of aqueous protein solutions using partial least squares methods. Biochemistry. 2004;43(9):2541-9.
38. Hosseini M, Schaffie M, Pazouki M, Darezereshki E, Ranjbar M. Biologically synthesized copper sulfide nanoparticles: production and characterization. Materials Science in Semiconductor Processing. 2012;15(2):222-5.
39. Karthik K, Jaya NV, Kanagaraj M, Arumugam S. Temperature-dependent magnetic anomalies of CuO nanoparticles. Solid state communications. 2011;151(7):564-8.
40. Padil VVT, Černík M. Green synthesis of copper oxide nanoparticles using gum karaya as a biotemplate and their antibacterial application. International journal of nanomedicine. 2013:889-98.
41. Yedurkar S, Maurya C, Mahanwar P. A biological approach for the synthesis of copper oxide nanoparticles by Ixora coccinea leaf extract. J Mater Environ Sci. 2017;8(4):1173-8.
42. Althamthami M, Temam EG, Temam HB, Hasan GG, Malfi N. Influence of hole-scavenger and different withdrawn speeds on photocatalytic activity of Co3O4 thin films under sunlight irradiation. Ceramics International. 2022;48(21):31570-8.